

Article

Distinguishing Amyloid Fibril Structures in Alzheimer's Disease (AD) by Two-Dimensional Ultraviolet (2DUV) Spectroscopy

Alfonso Ramon Lam, Jun Jiang, and Shaul Mukamel

Biochemistry, **Just Accepted Manuscript** • DOI: 10.1021/bi201317c • Publication Date (Web): 30 Sep 2011

Downloaded from <http://pubs.acs.org> on October 3, 2011

Just Accepted

"Just Accepted" manuscripts have been peer-reviewed and accepted for publication. They are posted online prior to technical editing, formatting for publication and author proofing. The American Chemical Society provides "Just Accepted" as a free service to the research community to expedite the dissemination of scientific material as soon as possible after acceptance. "Just Accepted" manuscripts appear in full in PDF format accompanied by an HTML abstract. "Just Accepted" manuscripts have been fully peer reviewed, but should not be considered the official version of record. They are accessible to all readers and citable by the Digital Object Identifier (DOI®). "Just Accepted" is an optional service offered to authors. Therefore, the "Just Accepted" Web site may not include all articles that will be published in the journal. After a manuscript is technically edited and formatted, it will be removed from the "Just Accepted" Web site and published as an ASAP article. Note that technical editing may introduce minor changes to the manuscript text and/or graphics which could affect content, and all legal disclaimers and ethical guidelines that apply to the journal pertain. ACS cannot be held responsible for errors or consequences arising from the use of information contained in these "Just Accepted" manuscripts.



ACS Publications
High quality. High impact.

**Distinguishing Amyloid Fibril Structures in
Alzheimer’s Disease (AD) by Two-Dimensional
Ultraviolet (2DUV) Spectroscopy**

A. R. Lam,* J. Jiang,* and S. Mukamel*

Department of Chemistry, University of California, Irvine, Irvine, CA 92697-2025 USA

E-mail: alamng@uci.edu; jiang1@uci.edu; smukamel@uci.edu

Phone: +1 949-824-6164. Fax: +1 949-824-4759

RUNNING HEADER: Distinguishing Amyloid Fibril Structures in Alzheimer’s Disease (AD)
by Two-Dimensional Ultraviolet (2DUV) Spectroscopy

*To whom correspondence should be addressed

Funding Information: National Institutes of Health (Grant GM059230 and GM091364) and National Science Foundation (Grant CHE-1058791)

Abstract

Understanding the aggregation mechanism of amyloid fibrils and characterizing their structures are important steps in the investigation of several neurodegenerative disorders associated with the misfolding of proteins. We report a simulation study of coherent two-dimensional chiral signals of three NMR structures of A β protein fibrils associated with Alzheimer's Disease: two models for A β (8–40) peptide wild-type (WT) and one for the Iowa (D23N) A β (15–40) mutant. Both far ultraviolet (FUV) signals ($\lambda = 190\text{--}250\text{ nm}$) which originate from the backbone $n\pi^*$ and $\pi\pi^*$ transitions, and near ultraviolet (NUV) signals ($\lambda \geq 250\text{ nm}$) associated with aromatic side-chains (Phe and Tyr) show distinct cross-peak patterns that can serve as novel signatures for the secondary structure.

Introduction

A large number of neurodegenerative diseases is linked to the formation and deposition of misfolded proteins to form amyloid fibrils. Probing the aggregation kinetics and fibril formation pathways had drawn a considerable experimental and computational effort (1–14). Alzheimer's Disease (AD) is a progressive neurodegenerative disorder whose pathology is characterized by the accumulation of senile plaques and neurofibrillar tangles in the brain. These plaques are made of fibrillar aggregates of the amyloid β -protein (A β). This protein comes from the cleavage of the amyloid precursor protein (APP) and is present in the body predominantly in two alloforms A β 40 and A β 42 which has two additional amino-acids in the C-terminal (15, 16).

Determination of the structure of amyloid fibrils is a challenging task. X-ray diffraction is a common tool used for the determination of global atomistic structures of proteins in crystals whereas nuclear magnetic resonance (NMR) techniques can yield structures in solution. The information

obtained from these conventional structural biology techniques is limited since amyloid fibrils are insoluble and do not crystallize. High-resolution molecular structure of amyloid fibrils is not available but geometrical models of amyloid fibrils based on solid NMR and others experimental data (17–20). Recent CD and NMR studies of A β monomers and dimers in solutions were used to characterize global properties such as secondary structures at different solutions concentrations, pH and temperatures (11, 21, 22). Ultraviolet (UV) spectroscopy provides an alternative structural tool. Both the peptide backbone and some side chains are active in this regime. The $n\pi^*$ and $\pi\pi^*$ transitions of the peptide backbone in the far ultraviolet (FUV) region ($\lambda = 190\text{--}250\text{ nm}$) and used for estimating secondary structure content. Circular dichroism (CD) spectroscopy in this region is a useful probe for protein secondary structures such as α -helices and β -strands. In the near ultraviolet (NUV) region ($\lambda \geq 250\text{ nm}$), aromatic side chains (Phe, Tyr, and Trp) usually provide more details about local interactions. Absorption and CD spectra of proteins are usually calculated using the Frenkel exciton matrix model which provides an efficient parametrization scheme for their electronic excitations (23–27).

Two-dimensional (2D) optical spectroscopy is a novel tool that can be used for structure refinement. Sequences of femtosecond laser pulses are employed to excite vibrational or electronic states and determine correlations between events which occur within two controlled time intervals. These correlations are displayed in two dimensional maps that reveal the molecular motions and fluctuating structures of a protein. These help to characterize local dynamics and determine intermediate states present in A β fibril formation process (28–31). Two-dimensional (2DIR) photon echo experiments combined with molecular dynamics simulations (MD) have been employed to test the quality of the MD methods and probe protein structures and fast folding processes. Previous simulation studies have demonstrated the potential of two-dimensional ultraviolet spectroscopy (2DUV) in the far and near UV regions for characterizing secondary structure in A β amyloid. A simulation protocol based on the Exciton Hamiltonian with Electrostatic Fluctuations (EHEF) was developed (32–34). The present computational study employs that protocol and is

1
2
3 aimed at demonstrating how the cross-peaks in chiral 2DUV signals may be used to distinguish
4
5 between three A β amyloid fibrils geometrical models suggested recently by the NMR studies of
6
7 Tycko and co-workers (17–20).
8
9

10
11 In Materials and Methods section, we explain the EHEF protocol, provide some technical details
12
13 and present the amyloid fibril models used. In Results and Discussion section, we present the one
14
15 and two-dimensional results for the near and far UV spectra. Finally, we provide the conclusions.
16
17
18
19

20 21 22 **Materials and Methods** 23 24

25 We consider the three A β peptides models shown in Figure 1. Models 1 and 2 correspond to the
26
27 A β (8–40) peptide with the sequence
28
29 GYEVHHQK¹⁶LVFFAE²²DVGSNKG³⁰IIGLMV³⁶GGVV⁴⁰. Model 1, first suggested by Petkova
30
31 *et al.* (18), consists of parallel β -sheets growing along the fibril growth axis. Model 2 which has
32
33 a three-fold symmetry about that axis is based on solid state NMR and electron microscopy per-
34
35 formed by Paravastu *et al.* (19). We used three peptides in each block making a three-fold sym-
36
37 metry complex composed by 9 peptides. Model 3 is the A β (15–40) segment of the above protein
38
39 with the point D23N mutation, known as the Iowa mutant. Its geometry consists of an anti-parallel
40
41 β -sheet growing along the fibril axis (20).
42
43
44
45

46 Molecular dynamics (MD) trajectories of the above models were obtained by using the NAMD
47
48 Package 2.7 (35) with the CHARMM27 force field (36). Simulations were carried out in aque-
49
50 ous solutions (TIP3P water model) with cubic periodic boundary conditions. The particle-mesh
51
52 Ewald (PME) protocol was used to calculate the long-range electrostatic interactions and a 12
53
54 cutoff distance was used for non-bonded interactions. 2.0 ns runs were used to minimize the pro-
55
56 teins at 300 K and 1250 MD snapshots were harvested for the 2DUV calculations. The 2DUV
57
58
59
60

spectra were computed using the EHEF protocol (32–34, 37) and the SPECTRON homemade program (38).

The simulated Linear Absorption (LA) and Circular Dichroism (CD) spectra in the entire UV regime ($\lambda = 180\text{--}250\text{ nm}$) for the three models are displayed in Figure 2 and Figure 3 respectively. We show the spectra of the side chain alone (black), the backbone (red), the additive spectrum (their sum in blue) and the total spectrum (green). The difference of the additive and the total spectrum shown in the right column in Figure 2 and Figure 3 indicates interactions between the backbone and side chains. The strongest differences are around 52000 cm^{-1} . The NUV region (above 250 nm) covers transitions of aromatic side chains (Phe, Tyr and Trp). Each has four valence electronic excitations known in Platt's notation as: 1L_a , 1L_b , 1B_a , and 1B_b . 1L_a and 1L_b which give the strong NUV peaks. The interactions of the aromatic residues may be used to characterize the structure. NUV signals of Model 1 have been studied earlier (34, 37). The FUV spectra (190–250 nm) originate from the peptide backbone $n\pi^*$ and $\pi\pi^*$ transitions and are sensitive to secondary structure as well. Even though aromatic residues are rare, their contributions to the FUV spectra are not much weaker than those of the backbone since they have larger transition dipole moments. The difference spectrum is much stronger for LA than CD. The CD backbone spectra in all models (Figure 3, red plots) show a clear FUV signatures of a typical β -strand conformation. In the coming sections, we shall analyze the NUV and FUV spectra in detail.

Results and Discussion

Near Ultraviolet (NUV) Signals

The simulated LA signals in the NUV regime for all three models are shown in Figure 4 (bottom). for Models 1 and 2. They exhibit sharp peaks around 37000 cm^{-1} while Model 3 only has a modest bump (indicated by green circle) at 38000 cm^{-1} . Another peak is observed in the 46000 cm^{-1}

for Model 1 and 2. This peak is missing in Model 3 due to its shorter sequence that does not have the Tyrosine Y9. We expect that a full sequence for Model 3 should show the aromatic side chain transitions at 46000 cm^{-1} .

The 2DNUV spectra computed with laser pulses centered at 37000 cm^{-1} and 3754 cm^{-1} bandwidth are displayed in Figure 5. All 2D spectra in this article are plotted on a nonlinear scale that interpolates between logarithmic for small values and linear for large values. It thus reveals both the strong and weak signals (34). The non-chiral *xxxx* signals (All pulses have parallel polarization) are shown in the top row. For Model 1, the signal is symmetric with respect to the diagonal. The 1L_b transitions dominate and show a negative diagonal peak (blue) centered at 37000 cm^{-1} . This is accompanied by two positive (red) side bands. The 1L_a transitions which originate from the coupling between the aromatic residues Phe and Tyr appear as a peak in Model 1 around 46000 cm^{-1} (blue), a weaker peak appear in than Model 2 and no peak is present in Model 3 where 1L_a transitions are invisible due to the lack of Tyrosine Y9. In Models 2 and 3, the 1L_b transitions shifted to 36000 cm^{-1} dominate with their respective side bands but Model 2 seems to have a weaker 1L_b transition than Models 1 and 3.

We next turn to chirality-induced signals. The CD spectra of all models shown in Figure 4 have aromatic side chain transition peaks at 37000 cm^{-1} and 46000 cm^{-1} . Model 3 also shows tiny peaks which could be attributed to aromatic side chain transition between Phe of a peptide with the other Phe in another peptide on the same layer.

The chirality-induced *xxxy* 2DUV signal of Model 1, where the last pulse is polarized perpendicular to the other three (bottom row in Figure 5) is non-symmetric with respect to the diagonal. The 1L_b and 1L_a transitions appear as two positive (red) peaks with their negative side bands centered around at 37000 cm^{-1} and 46000 cm^{-1} , respectively. The 1L_b peak has a strong side band in the lower triangle, shifted from the diagonal while a similar pattern is seen in the upper side band of

the 1L_a transition peak. This indicates that the 1L_b and 1L_a transitions are coupled. The signals of Model 2 and 3 are very different from Model 1. Both are symmetric but with different intensities. The 1L_b transition of Model 2 is stronger than in Model 3. This may be due to the nearest-neighbor interactions between Phe in the $A\beta$ peptides in Model 2 that exist also in Model 1. 1L_a is weak in models 2 and 3, suggesting weak coupling between 1L_b and 1L_a transitions. A possible explanation could be the fact that intermolecular interactions of aromatic residues Phe-Tyr, ie Phe and Tyr interact each other in one $A\beta$ peptide in a given layer, and generates coupling between 1L_b and 1L_a transitions. The geometry of Model 2 allows Tyr to interact with the Phe of another $A\beta$ peptide in another layer. Our previous 2DNUV studies of the amyloid fibril growth in Model 1 (39) showed how the intensities in the signals correlate with the complex size. Intramolecular interaction of aromatic residues Phe-Tyr in one $A\beta$ peptide is seen only in Model 1 while aromatic residue couplings are missed in Model 3 which lacks the Tyr residue (Y9) in its sequence.

In order to trace the origin of these spectral features, we have computed the transition populations. These are defined as the squares of the exciton wave function expansion coefficients, in the basis of the local amide excitations and are displayed in Figure 6. We see that the NUV $xxxy$ signals (bottom row in Figure 5) of all models are induced by the aromatic residues (Phe and Tyr) and are well localized in the sequence. In Model 2, 1L_b transitions is observed as a red peak in the 34000–36000 cm^{-1} region but no coupling (perhaps very weak) between 1L_b and 1L_a transitions are observed in the 44000–46000 cm^{-1} region. Model 3 shows a blue peak at 34000–36000 cm^{-1} region while models 1 and 2 have red peaks that can be ascribed to the complex geometry since it has only Phe–Phe intermolecular interactions between two peptides. Similarly, the 44000–46000 cm^{-1} region shows signals for Models 1 and 2 and not in Model 3.

Far Ultraviolet (FUV) Signals

The simulated LA and CD spectra of the three A β peptide amyloid fibril models in the FUV region are shown in Figure 7. All spectra are similar with peaks centered around at 52000 cm^{-1} . The 2DFUV spectra generated by laser pulses centered at 52000 cm^{-1} and bandwidth at 3754 cm^{-1} are displayed in Figure 8. The non-chiral 2DUV $xxxx$ spectra (top row) show the characteristic features of a β -sheet: a weak peak centered around at 52000 cm^{-1} on the diagonal maps ($\Omega_3 = -\Omega_1$) for all three models.

We next turn to the chiral signals. The CD signals are distinguishable and have the characteristic of a β -strand rich-structure profile, in agreement with experiments (21, 22, 40). Model 1 has stronger CD signals in the region 50000–54000 cm^{-1} whereas signal for models 2 and 3 show peaks around 50000 cm^{-1} and decay beyond 52000 cm^{-1} . The ($xxxy$) chiral 2DUV signals are much richer than the $xxxx$ spectra (Figure 8, bottom row). Model 1 has a symmetric strong peak at 52000 cm^{-1} . Models 2 and 3 show a symmetric butterfly-like spectra with a positive peak near 52000 cm^{-1} and a negative peak at 54000 cm^{-1} . Model 3 has an additional positive peak near 57000 cm^{-1} . The transition populations in the FUV regime are displayed in Figure 9. These reveal that at 52000 cm^{-1} , the signals for all three models come from the electronic transition of all peptide groups and reflect the strongest peak of the CD spectra (See Figure 9 top row and Figure 9 left column). At 54000 cm^{-1} , weak contributions from the backbone are seen only in Model 1 CD and LA spectra. In contrast, that region shows a broad feature that overlaps with the 52000 cm^{-1} peak (Figure 9 top row left panel). The middle column in Figure 9 shows that this is mainly due to interactions between the turn loop of a A β peptide located in a β -sheet layer with the terminal of a A β peptide located in the other β -sheet layer. The 2DUV signals of models 2 and 3 are different. They show an additional weak peak at 54000 cm^{-1} on the 2DFUV spectra originating from the interactions between turns-ends between different fibrils layers. The CD spectra of both models in the 52000 cm^{-1} and 54000 cm^{-1} regime are different. We expect a similar 2DUV spectrum to Models 1 and 3 since their global geometry consists in a β -sheet layer with alternate loops between A β peptides.

However, the two show significant differences. The 2DFUV spectra (Figure 8 lower-right plot) shows also a butterfly-like spectrum as in Model 2, indicating that in addition to the interactions between turns of a $A\beta$ peptide from a β -sheet layer with the ends of a $A\beta$ peptide from another β -sheet layer as in Model 2, the complex geometry is important as well. Both models show interactions between turn and termini among peptides. In Model 2, these are between stacks while in Model 3 they are among peptides in the same stack. This could be the origin of the butterfly shape of 2DFUV signal.

Conclusions

We have employed the EHEF protocol to predict the 2DUV spectra of three amyloid fibril structure models proposed by Tycko and collaborators. The 1D (CD and LA) spectra of the three models suggest that the side chains and backbone transitions are coupled. 2DUV spectra of the aromatic side chains show clear signatures of 1L_b and 1L_a transitions and their respective couplings in all models. The 2DFUV chirality-induced $xxxy$ signals associated with aromatic residue couplings between transitions can describe the variations of interactions between residues which strongly depend on the complex geometry. The 1L_b and 1L_a couplings can be hidden in the 2DFUV maps by either intermolecular interactions of aromatic residues Phe-Tyr as seen in Model 2 or there is a correlation between number of peptides in a $A\beta$ sheet with the 2DUV intensity. Since the sequence of the Iowa mutant $A\beta$ peptide shown in Model 3 was shorter, the 1L_b and 1L_a transitions were undetectable. However, its geometry (peptides forming an anti-parallel β -strand sheets) had resulted in a butterfly-like chiral-induced signals in the FUV similar to Model 2.

Acknowledgement

We wish to thank Dr. Robert Tycko for providing the three A β amyloid models.

References

1. Walsh, D. M., Lomakin, A., Benedek, G. B., Condron, M. M., and Teplow, D. (1997) Amyloid β -protein fibrillogenesis: detection of a protofibrillar intermediate. *J. Biol. Chem.* 272, 22364–22372.
2. Kirkitadze, M. D., Bitan, G., and Teplow, D. B. (2002) Paradigm shifts in Alzheimer's Disease and other degenerative disorders: the emerging role of the oligomers assemblies. *J. Neurosci. Res.* 69, 567–577.
3. Nostrand, W. E. V., Melchor, J. P., Cho, H. S., Greenberg, S. M., and Rebeck, G. W. (2001) Pathogenic Effects of D23N Iowa Mutant Amyloid β -Protein. *J. Biol. Chem.* 276, 32860–32866.
4. Crescenzi, O., Tomaselli, S., Guerrini, R., Salvatori, S., D'Ursi, A. M., Temussi, P. A., and Picone, D. (2002) Solution structure of the Alzheimer amyloid β -peptide (1–42) in an apolar microenvironment. Similarity with a virus fusion domain. *Eur. J. Biochem.* 269, 5642–5648.
5. Bitan, G., Kirkitadze, M. D., Lomakin, A., Vollers, S. S., Benedek, G. B., and Teplow, D. B. (2003) Amyloid β -protein ($A\beta$) assembly: $A\beta$ 40 and $A\beta$ 42 oligomerize through distinct pathways. *Proc. Natl. Acad. Sci. USA* 100, 330–335.
6. Urbanc, B., Cruz, L., Yun, S., Buldyrev, S. V., Bitan, G., Teplow, D. B., and Stanley, H. E. (2004) *In silico* study of amyloid β -protein ($A\beta$) folding and oligomerization. *Proc. Natl. Acad. Sci. USA* 101, 17345–17350.
7. Glabe, C. G. (2005) Amyloid accumulation and pathogenesis of Alzheimer's disease: significance of monomeric, oligomeric and fibrillar $A\beta$. *Subcell Biochem.* 38, 167–177.
8. Lazo, N. D., Grant, M. A., Condron, M. C., Rigby, A. C., and Teplow, D. B. (2005) On the nucleation of amyloid β -protein monomer folding. *Prot. Sci.* 14(6), 1581–1596.

9. Xu, Y., Shen, J., Luo, X., Zhu, W., Chen, K., Ma, J., and Jiang, H. (2005) Conformational Transition of Amyloid β -peptide. *Proc. Natl. Acad. Sci. USA* 102, 5403–5407.
10. Baumketner, A., Bernstein, S. L., Wyttenbach, T., Bitan, G., Teplow, D. B., Bowers, M. T., and Shea, J.-E. (2006) Amyloid β -protein monomer structure: a computational and experimental study. *Prot. Sci.* 15, 420–428.
11. Lim, K. H., Collver, H. H., Le, Y. T. H., Nagchowdhuri, P., and Kenney, J. M. (2006) Characterization of distinct amyloidogenic conformations of the A β (1-40) and A β (1-42) peptides. *Biochem. and Biophys. Res. Com.* 353, 443–449.
12. Teplow, D. B. (2006) Preparation of amyloid β -protein for structural and functional studies. *Methods. Enzymol.* 413, 20–33.
13. Grant, M. A., Lazo, N. D., Lomakin, A., Condrón, M. M., Arai, H., Yamin, G., Rigby, A. C., and Teplow, D. B. (2007) Familial Alzheimer's disease mutations alter the stability of the amyloid β -protein monomer folding nucleus. *Proc. Natl. Acad. Sci. USA* 104(42), 16522–16527.
14. Lam, A. R., Teplow, D. B., Stanley, H. E., and Urbanc, B. (2008) Effects of the Arctic (E22)-> G) Mutation on Amyloid β -Protein Folding: Discrete Molecular Dynamics Study. *J. Am. Chem. Soc.* 130(51), 17413–17422.
15. Hardy, J., and Selkoe, D. J. (2002) The amyloid hypothesis of Alzheimer's disease: Progress and problems on the road to therapeutics. *Science* 297, 353–356.
16. Hardy, J. (2002) Testing times for the "amyloid cascade hypothesis". *Neurobiol. Aging* 23, 1073–1074.
17. Petkova, A. T., Ishii, Y., Balbach, J. J., Antzutkin, O. N., Leapman, R. D., Delaglio, F., and Tycko, R. (2002) A Structural Model for Alzheimer's β -Amyloid Fibrils Based on Experimental Constraints from Solid State NMR. *Proc. Natl. Acad. Sci. USA* 99, 16742–16747.

18. Petkova, A. T., Yau, W. M., and Tycko, R. (2006) Experimental Constraint on Quaternary Structure in Alzheimer's β -Amyloid Fibrils. *Biochemistry* 45, 598–512.
19. Paravastu, A., Leapman, R. D., Yau, W. M., and Tycko, R. (2008) Molecular Structural Basis for Polymorphism in Alzheimer's β -Amyloid Fibrils. *PNAS* 105, 18349–18354.
20. Tycko, R., Sciarretta, K. L., Orgel, J. P. R. O., and Meredith, S. C. (2009) Evidence for Novel β -Sheet Structures in Iowa Mutant β -Amyloid Fibrils. *Biochemistry* 48(26), 6072–6084.
21. Barrow, C. J., A., Y., Kenny, P. T. M., and Zagorski, M. G. (1992) Solution Conformations and Aggregational Properties of Synthetic Amyloid β -Peptides of Alzheimer's Disease: Analysis of Circular Dichroism Spectra. *J. Mol. Biol.* 225(4), 1075–1093.
22. Gursky, O., and Aleshkov, S. (2000) Temperature-dependent β -sheet formation in beta-amyloid A β_{1-40} peptide in water: Uncoupling β -structure folding from aggregation. *Biochim. Biophys. Acta.* 1476, 93–102.
23. Frenkel, J. (1931) On the Transformation of Light into Heat in Solids. I. *Physical Review* 37, 17–44.
24. Besley, N. A., and Hirst, J. D. (1999) Theoretical Studies toward Quantitative Protein Circular Dichroism Calculations. *J. Am. Chem. Soc.* 121(41), 9636–9644.
25. Woody, R. W. (2005) The Exciton Model and the Circular Dichroism of Polypeptides. *Monatsh. Chem.* 136(3), 347–366.
26. Bulheller, B. M., Rodger, A., and Hirst, J. D. (2007) Circular and Linear Dichroism of Proteins. *Phys. Chem. Chem. Phys.* 9, 2020–2035.
27. Abramavicius, D., Palmieri, B., Voronine, D. V., Sanda, F., and Mukamel, S. (2009) Coherent Multidimensional Optical Spectroscopy of Excitons in Molecular Aggregates; Quasiparticle versus Supermolecule Perspectives. *Chemical Review* 109(6), 2350–2408.

- 1
2
3
4
5
6
7
8
9
10
11
12
13
14
15
16
17
18
19
20
21
22
23
24
25
26
27
28
29
30
31
32
33
34
35
36
37
38
39
40
41
42
43
44
45
46
47
48
49
50
51
52
53
54
55
56
57
58
59
60
28. Smith, A. W., and Tokmakoff, A. (2007) Amide I two-dimensional infrared spectroscopy of β -hairpin peptides. *J. Chem. Phys.* 125, 045109–1–10.
29. Kim, Y. S., Liu, L., Axelsen, P. H., and Hochstrasser, R. M. (2008) Two-dimensional Infrared Spectra of Isotopically Diluted Amyloid Fibrils from A β 40. *Proc. Natl. Acad. Sci. USA* 105(22), 7720–7725.
30. Strasfeld, D. B., Ling, Y. L., Shim, S.-H., and Zanni, M. T. (2008) Tracking Fiber Formation in Human Islet Amyloid Polypeptide with Automated 2D-IR Spectroscopy. *J. Am. Chem. Soc.* 130, 6698–6699.
31. Shim, S.-H., Gupta, R., Ling, Y. L., Strasfeld, D. B., Raleigh, D. P., and Zanni, M. T. (2009) Two-dimensional IR spectroscopy and isotope labeling defines the pathway of amyloid formation with residue-specific resolution. *Proc. Natl. Acad. Sci. USA* 106(16), 6614–6619.
32. Jiang, J., Abramavicius, D., Bulheller, B. M., Hirst, J. D., and Mukamel, S. (2010) Ultraviolet Spectroscopy of Protein Backbone Transitions in Aqueous Solution: Combined QM and MM Simulations. *J. Phys. Chem. B* 114, 8270–8277.
33. Jiang, J., and Mukamel, S. (2010) Two-Dimensional Ultraviolet (2DUV) Spectroscopic Tools for Identifying Fibrillation Propensity of Protein Residue Sequences. *Ang. Chem.* 49(50), 9666–9669.
34. Jiang, J., and Mukamel, S. (2011) Two-Dimensional Near-Ultraviolet Spectroscopy of Aromatic Residues in Amyloid Fibrils: A First Principles Study. *Phys. Chem. Chem. Phys.* 13, 2394–2400.
35. Phillips, J. C., R. Braun, W. W., Gumbart, J., Tajkhorshid, E., Villa, E., Chipot, C., Skeel, R. D., Kalé, L., and Schulten, K. (2005) Scalable Molecular Dynamics with NAMD. *J. Comp. Chem.* 26(16), 1781–1802.

1
2
3
4
5
6
7
8
9
10
11
12
13
14
15
16
17
18
19
20
21
22
23
24
25
26
27
28
29
30
31
32
33
34
35
36
37
38
39
40
41
42
43
44
45
46
47
48
49
50
51
52
53
54
55
56
57
58
59
60

36. MacKerell, A. D. *et al.*. (1998) All-Atom Empirical Potential for Molecular Modeling and Dynamics Studies of Proteins. *J. Comp. Chem.* 102, 3586–3616.

37. Jiang, J., Abramavicius, D., Falvo, C., Bulheller, B. M., Hirst, J. D., and Mukamel, S. (2010) Simulation of Two Dimensional Ultraviolet (2DUV) Spectroscopy of Amyloid Fibrils. *J. Phys. Chem. B* 114, 12150–12156.

38. Zhuang, W., Abramavicius, D., and Mukamel, S. (2005) Dissecting Coherent Vibrational Spectra of Small Proteins into Secondary Structural Elements by Sensitivity Analysis. *Proc. Natl. Acad. Sci. USA* 102(7), 7443–7448.

39. Jiang, J., and Mukamel, S. (2011) Probing Amyloid Fibril Growth by Two-Dimensional Near-Ultraviolet Spectroscopy. *J. Phys. Chem. B* 115, 6321–6328.

40. Van Nostrand, W. E., Melchor, J. P., and Ruffini, L. (1998) Pathologic amyloid β -protein cell surface fibril assembly on cultured human cerebrovascular smooth muscle cells. *Journal of Neurochemistry* 70(1), 216–223.

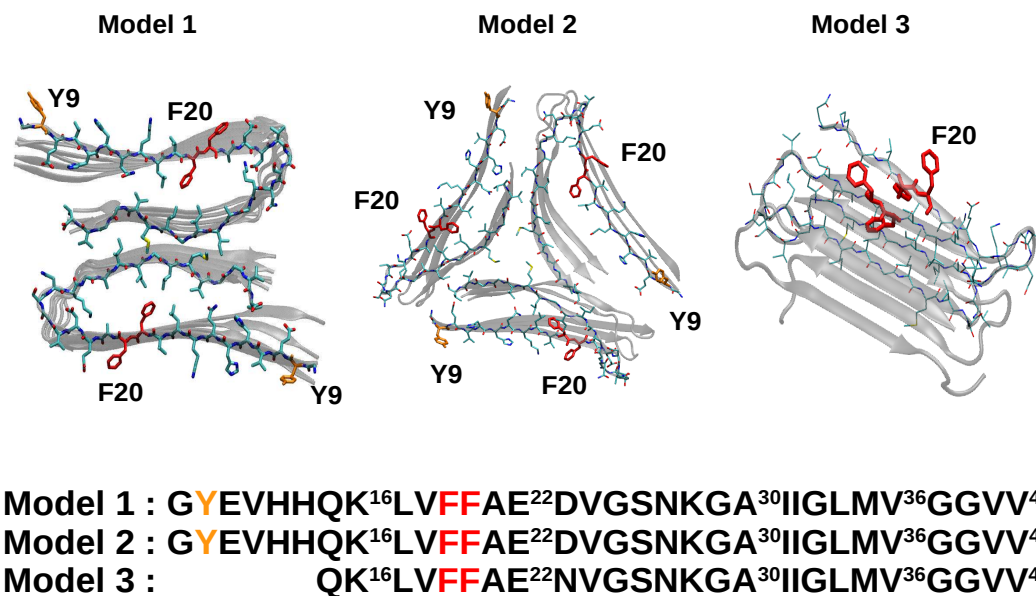


Figure 1: Structure and sequence of the three A β amyloid fibril models reported by Tycko and co-workers (18–20). The aromatic residues are marked: Phenylalanine (red); and Tyrosine (orange).

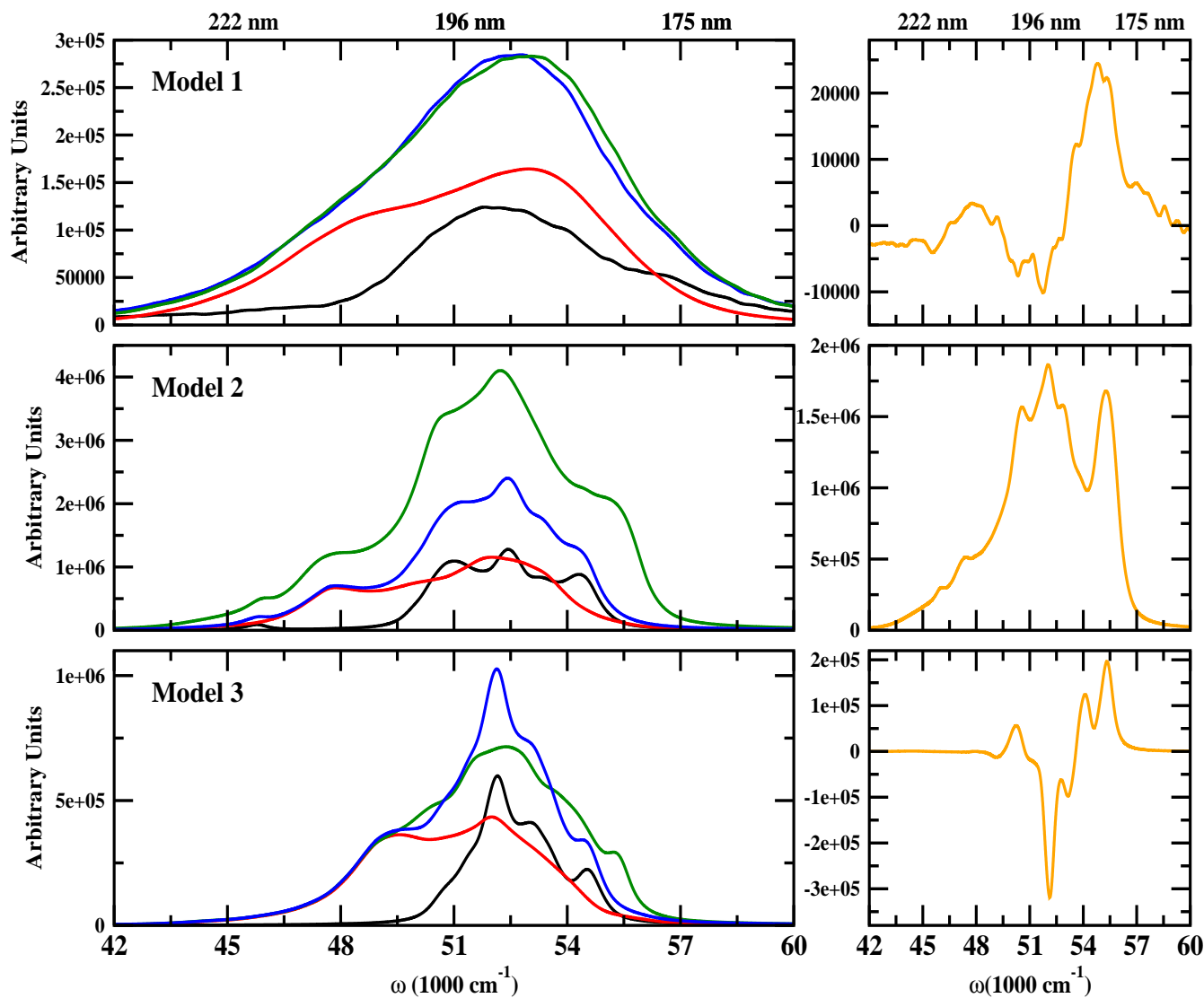


Figure 2: Left column: Simulated LA spectra. Total signal (green), backbone alone (red), side chain alone (black), additive spectrum (backbone + side chain) (blue). Right column: Difference of the Total and the Additive LA spectra (orange)

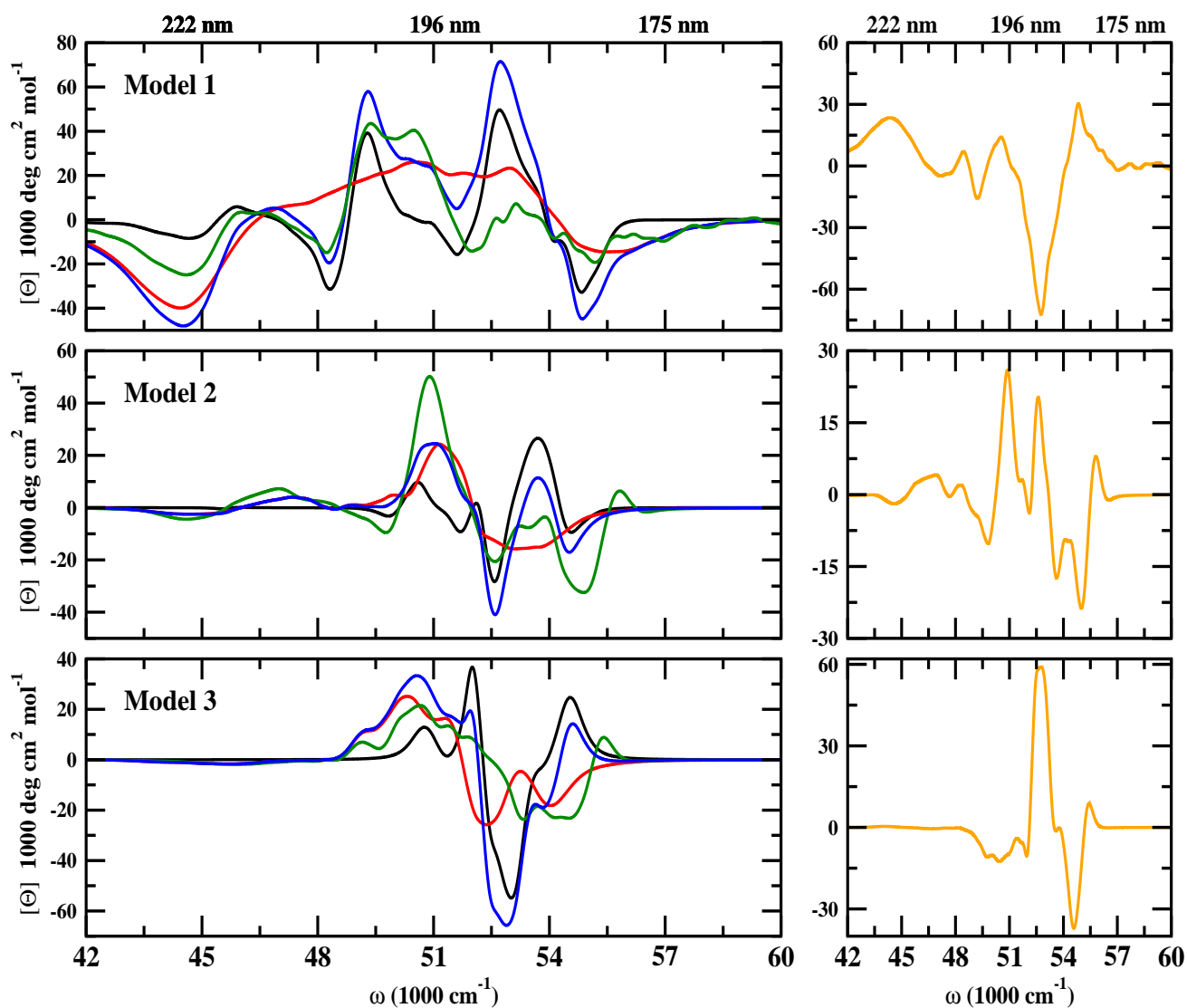


Figure 3: Same as in Figure 2 but for CD spectra

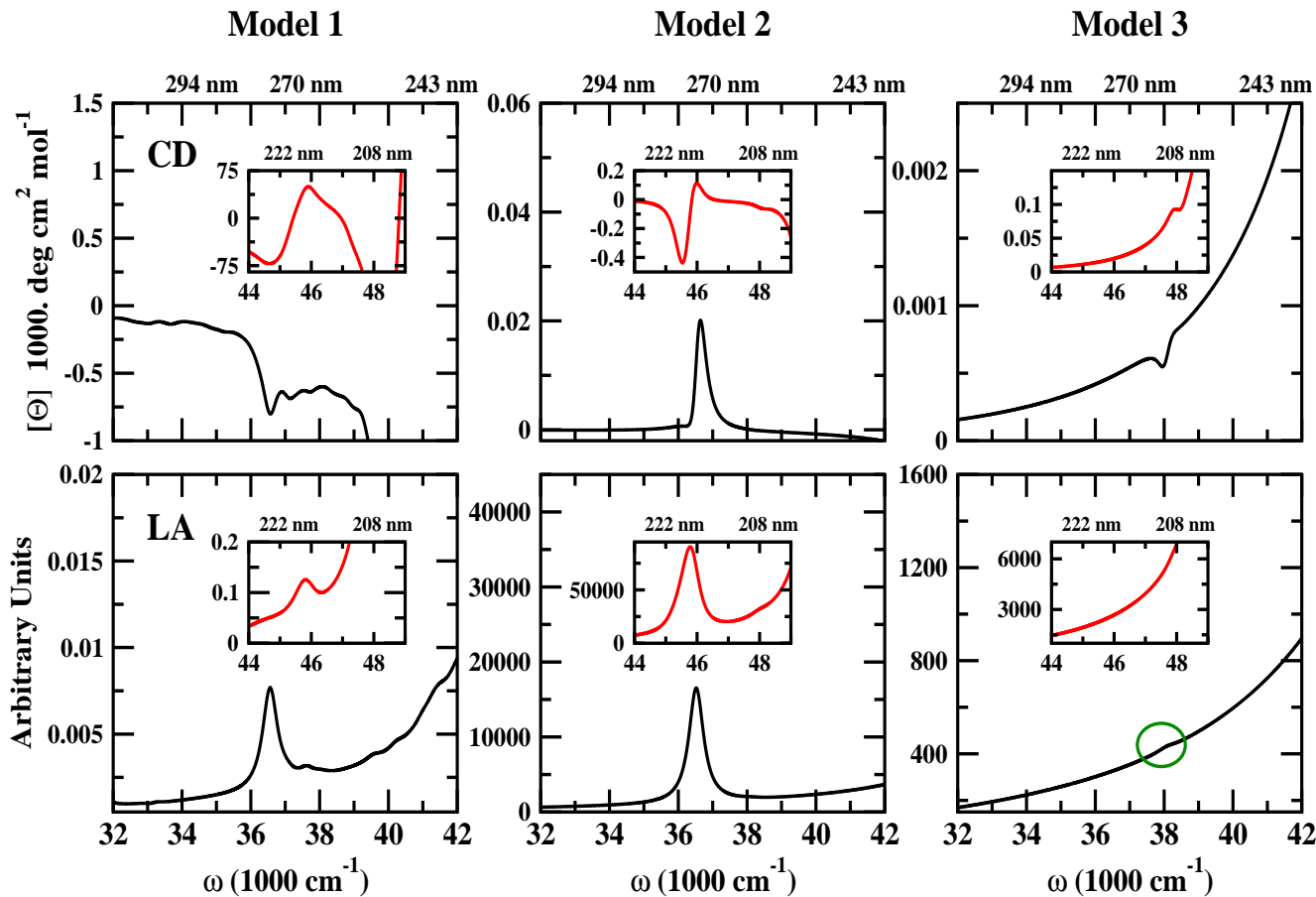


Figure 4: Simulated NUV CD (top row) and linear absorption (LA) (bottom row) of the three Aβ amyloid models. Inserts show the region [44000, 48000] cm^{-1} .

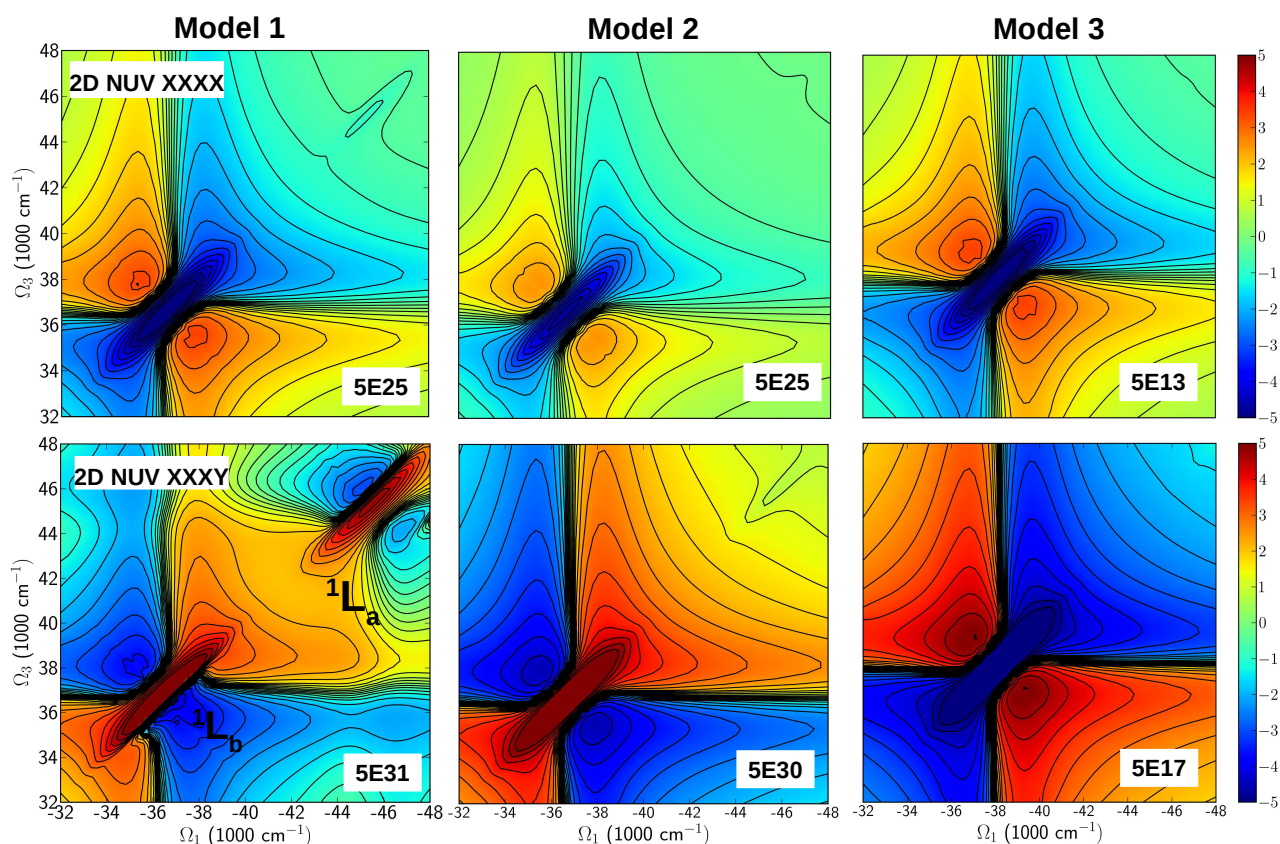


Figure 5: Simulated 2DNUV photon echo signals of the three $A\beta$ amyloid models. **Top row:** The non-chiral (xxxx) polarization configuration. The signals show a similar pattern but different intensities. Peaks centered at 37000 cm^{-1} is similar in intensity for Models 1 and 2 while in Model 3 is shifted away from the center and less intense. **Bottom row:** chirality induced (xxxy) polarization configuration. The spectra show some differences in the 1L_b region (37000 cm^{-1}). Model 1 has a strong 1L_a transition at 46000 cm^{-1} while in Model 2 is weaker. Spectra are displayed on the non-linear scale as defined in ref. (34). The s parameter is shown at the bottom right of each panel.

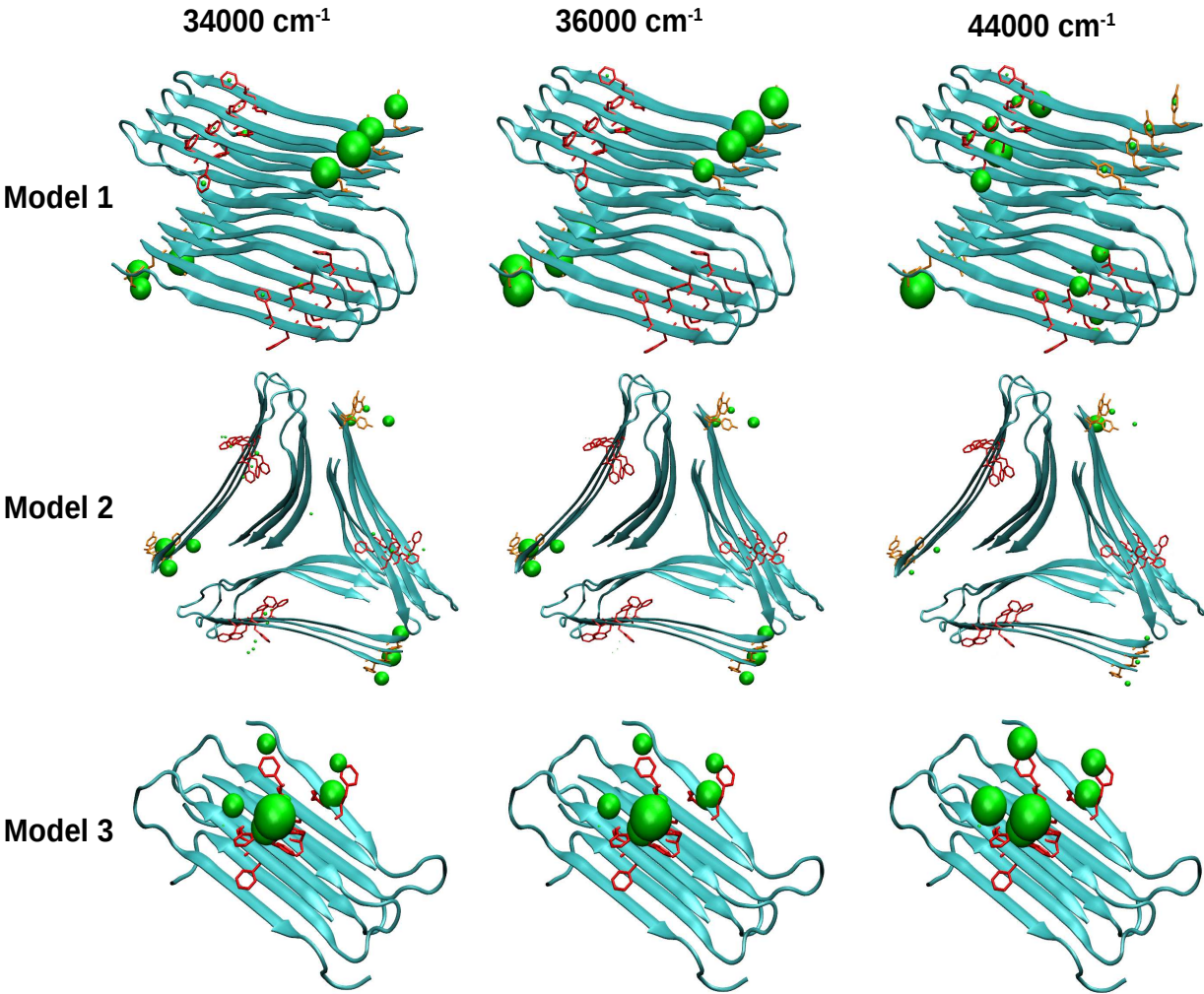


Figure 6: Transition populations for three NUV spectral regimes of the A β amyloid fibril models.

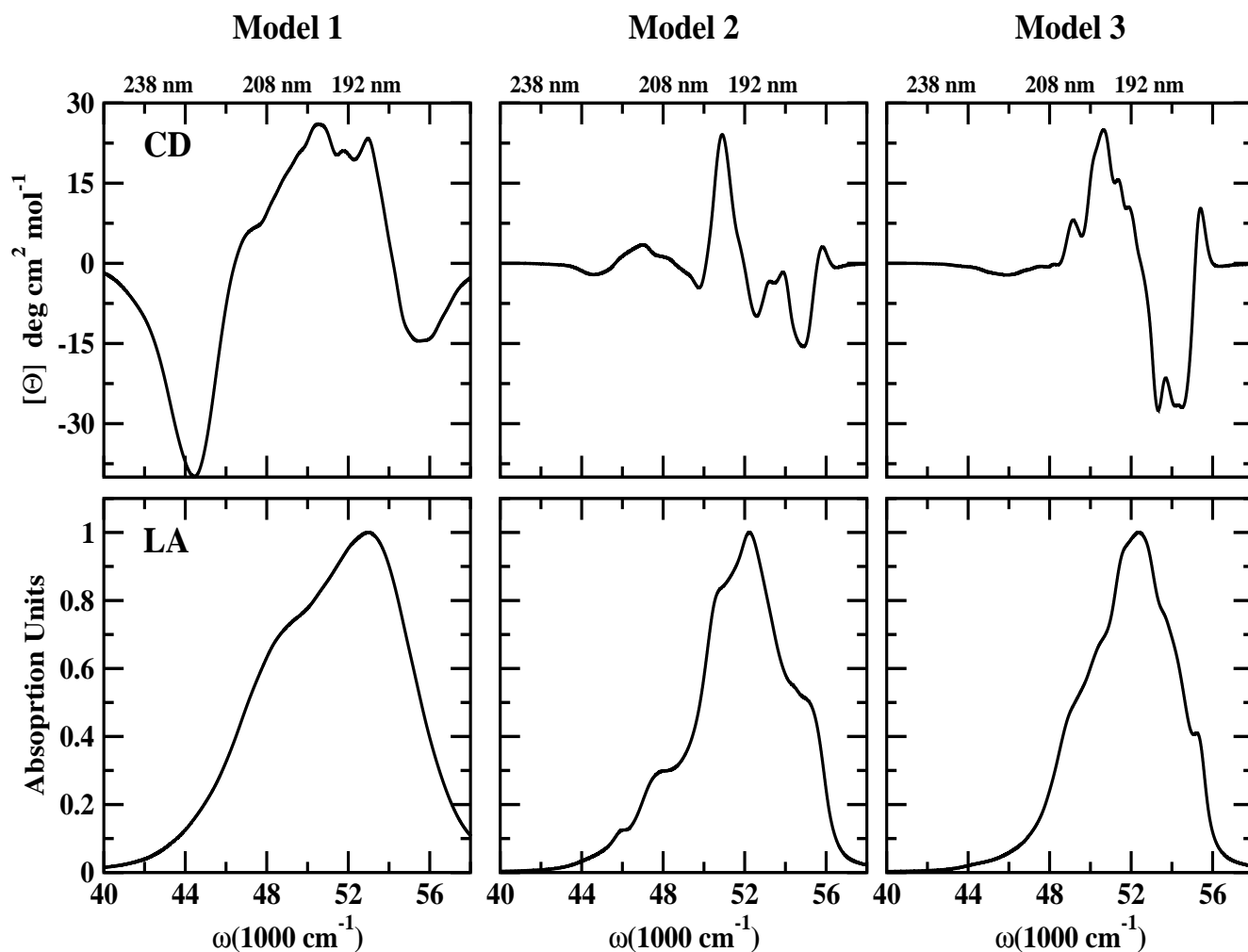


Figure 7: Simulated FUV CD (top row) and linear absorption (LA) spectra (bottom row) of the three A β amyloid models.

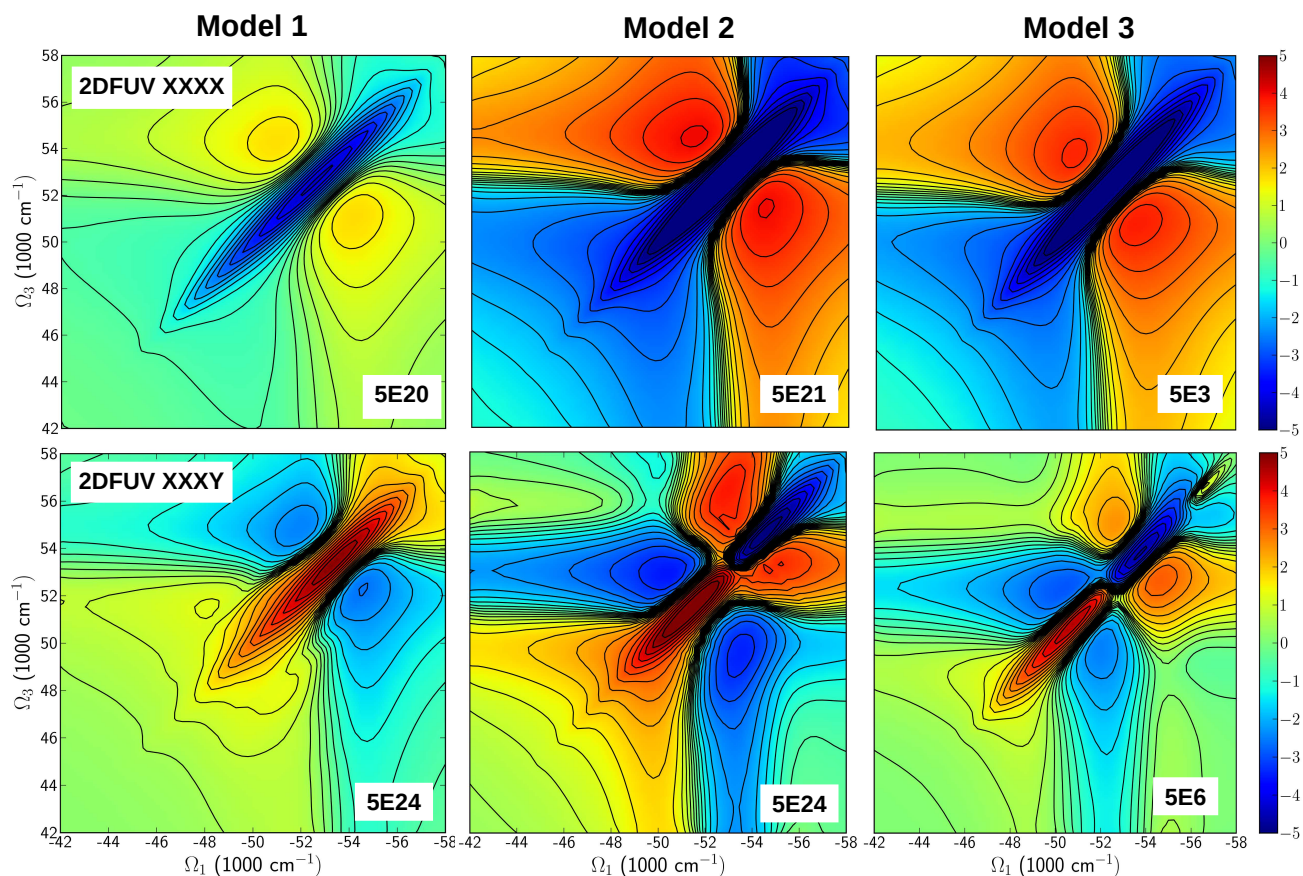


Figure 8: Same as in Figure 5 but for the 2DFUV regime. **Top row:** The non-chiral (xxxx) polarization configuration. All models display similar pattern but different intensities. **Bottom row:** chirality induced (xxxy) polarization configuration. Model 1 displays a strong peak at 52000 cm^{-1} while in Models 2 and 3 display butterfly-like shapes with two peaks in the 50000 cm^{-1} to 54000 cm^{-1} regime. Model 3 shows a small additional peak at 57000 cm^{-1} .

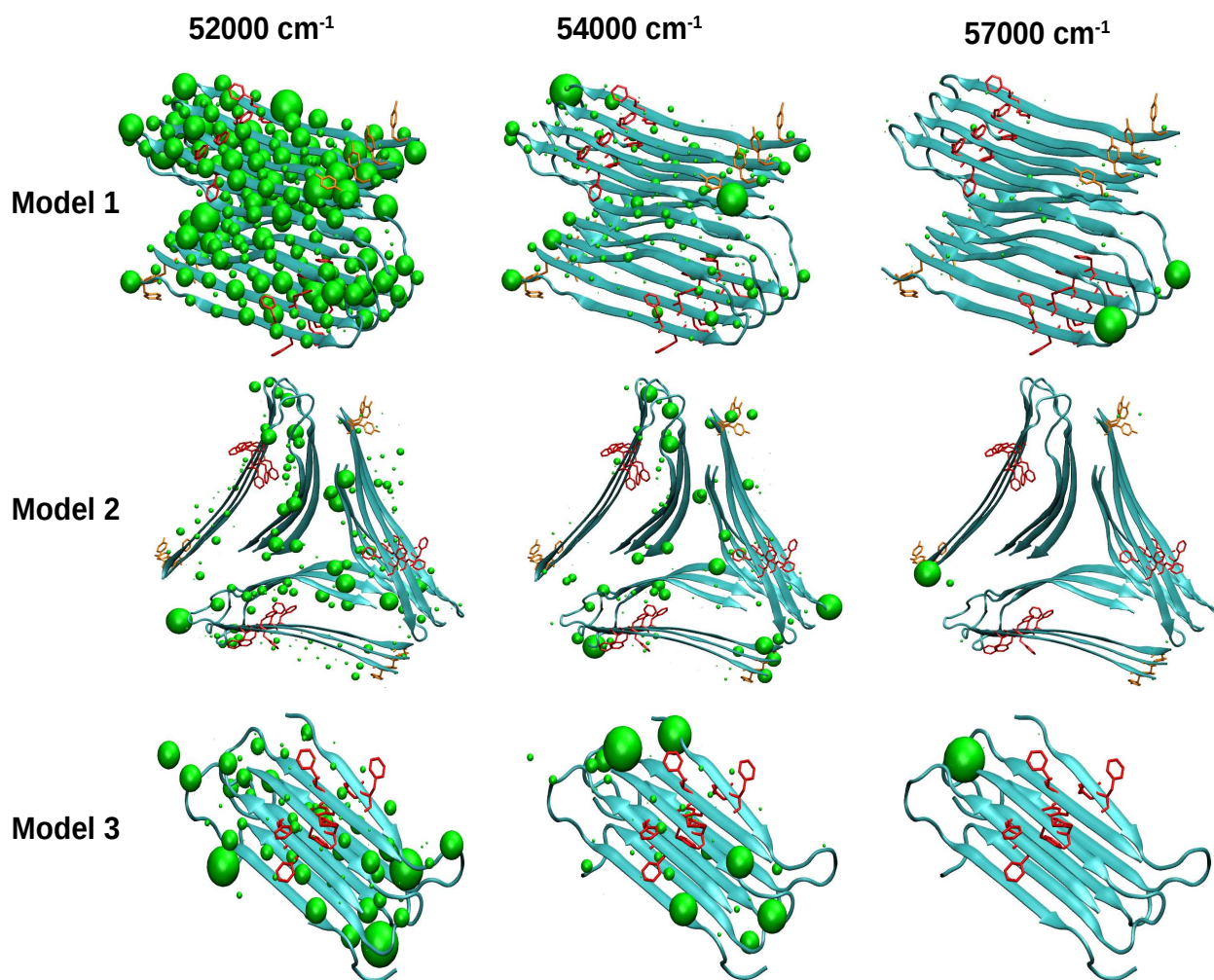


Figure 9: Transition populations for three FUV spectral regimes of the A β amyloid fibril models.

Image for Table of Content

